Subsurface Microstructure Evolution and Residual Stress in 42CrMo4 Steel after Single-Pass Pendulum Tests

Janis S. Kimm
Ruhr-Universität Bochum, Bochum, Germany
Email: kimm@wtech.rub.de

Fabian Pöhl[1], Petra Wiederkehr[2] and Werner Theisen[1]
[1]Ruhr-Universität Bochum, Universitätsstraße 150, 44801 Bochum, Germany
[2]Technische Universität Dortmund, Emil-Figge-Straße 50, 44227 Dortmund, Germany

***Abstract*— This work investigates the effect of cutting on the microstructure and subsurface properties of a cut specimen, with particular focus on the influence of the sample's microstructure and its evolution. Single-pass pendulum tests were conducted with samples of 42CrMo4 steel that had been subjected to different heat treatments. The subsurface region after cutting was analyzed optically by SEM and EBSD. The strain hardened surface region was investigated by nanoindentation. It was found that a soft-annealed structure, in particular, was altered deeply by cutting, resulting in a hardness increase as well as an microstructure that is elongated and refined by high shear deformation microstructure in near-surface regions. The strain hardening behavior and potential of a microstructure had a striking influence on the subsurface alteration. Although some microstructures yielded the same forces under equal cutting conditions, the subsurface alteration was different. This type of change in microstructure was correlated with the micromechanical properties and residual stresses. General influences, such as cutting depth, on the alteration of microstructures by cutting were also taken into account.**

***Index Terms*—machining, subsurface microstructure, residual stress, nanoindentation, EBSD**

I. Introduction

Machining production is the most commonly used means to produce final contours and surfaces of industrial and consumer goods. In times of a new industrial revolution, with high demands for adaptability to meet ever-changing needs in production, the predictability and computability of cutting processes is of enormous interest for industry and research [1].Particularly the production of thin walls and other hardly machinable geometries in small lots as well as further challenges for production such as chatter marks and vibrations, justify intensive research efforts. A major part of research projects concerning machining are related to the measurement of process forces and chip forms and this is often coupled with simulations to find better ways to predict machining processes [2–7]. However, for a complete description of a machining process, it is essential to consider the microstructural influences on the cut workpiece. For simplification, workpieces are often treated like a uniform and isotropic continuum that is defined by its hardness and chemical composition only. The possible variety of macroscopic and microscopic properties that a heat treatment could establish in steels and how they affect cutting also needs to be taken into account.

Microstructural alteration caused by cutting was analyzed, for instance, by TODAKA et al. for the case of drilled holes in a martensitic and a ferritic-pearlitic steel [8]. A nanocrystalline zone formed around the drilled hole and into the bulk material. This was followed by a severely sheared region. The hardness was found to increase towards the surface; however, because two different steels were used, a direct comparison of only the microstructural influence was not possible. Nevertheless, the massive shearing that a microstructure endures during machining operation was observed well in the etched ferritic-pearlitic subsurface region. In the field of hard turning, the formation of white etching layers has been the topic of research projects, and the focus was often set towards the temperature and mechanical stresses in the contact zone and thus the mechanisms of deformed or transformed white layer formation [9–14]. The intentional creation of severely deformed surface areas has already been performed by sliding wear experiments and severe plastic deformation that provoke similar mechanisms, but are not related to real deformations during machining [15,16]. Another important part of the workpiece alteration during cutting processes are the residual stresses inside the material. They can influence the consequent cuts and cause unwanted deformation of thin-walled products and may even influence product lifetime and corrosion resistance [17–19]. This research discusses how the precut microstructural conditions influence machining-induced subsurface alteration and what the

Manuscript received December 8, 2019; revised July 5, 2020.
Project number: Mercur foundation (PE-216-0024) Virtual Machining;

doi: 10.18178/ijmerr.9.8.1072-1080

alteration looks like, which has yet not received much attention in the literature.

II. Experimental Process

A. Examined Material And Heat Treatments

To cover a wide range of microstructures, the low-alloyed tempering steel 42CrMo4 (AISI 4140) (chemical composition: 0.429% C, 0.225% Si, 0.757% Mn, 0.014% P, 0.02% S, 1.101% Cr, 0.188% Mo) was heat-treated to four different states. The decarbonized layer was removed after heat treatment when the sample geometry, including the bar on the top, was machined. One of the investigated microstructures in the cutting experiments was a hardened state (hereinafter referred to as "H"). The workpiece was austenitised at 850 ℃ and quenched in water. After hardening, a hardness of 660 HV was measured and the microscope images reveal a typical acicular martensitic microstructure (Fig.1a). Two quenched-and-tempered states were created: quenched and subsequently tempered at 540 ℃ and 660 ℃ respectively for two hours ("QT540" and "QT660", Fig. 1b and 1c, respectively). The QT540 still has a needle-like microstructure, but tempering carbides have formed and the relaxed martensite has a hardness of around 390 HV. In QT660 the needles are no longer visible and even more carbides are formed, whereas the hardness is 300 HV. The fourth microstructure was established by soft annealing for four hours at 700 °C ("SA"). In comparison to the QT states, the carbides grew visibly (Fig. 1d) and the hardness dropped to 250 HV. The heat treatments of the steel with the same chemical composition and from the same lot produced a variety of macroscopic properties such as hardness and strength. Quasistatic tensile tests at room temperature were used to measure macroscopic properties to provide a basis for comparison (Table I). The martensitic, quenched-only samples have the highest strengths and lowest elongations. Higher and longer heat-treatment times and temperatures increased the elongation in the order QT540, QT660 and SA, but decreased the strength.

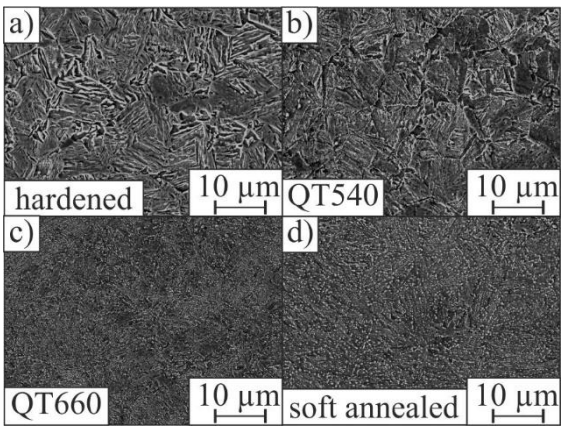

Figure 1. Microstructures of a) hardened, quenched and tempered steel at b) 540 ℃ and c) 660 ℃ and d) soft-annealed.

TABLE I. Macroscopic Properties of All Differently Heat-Treated Samples from Quasistatic Tensile Tests.

Heat treatment / Properties	Hardened	QT540	QT660	Soft Annealed
Hardness [HV30]	660	376	302	252
Proof strength [MPa]	1376	1213	831	637
Ultimate strength [MPa]	2345	1288	928	759
Uniform elongation [%]	4.1	4.2	6.9	9.3
Ultimate elongation [%]	6.0	12.5	17.9	21.1

B. Cutting Experiments

Cutting experiments were conducted with a single-pass pendulum. The pendulum was self-built from an impact tester for Charpy tests (Fig. 2a). Bar samples were clamped into a holder on a force-measurement platform that was adjustable in height to vary the uncut chip thickness (Fig. 2b). For the experiments, the arm was cranked up to 135 ° and released so that the cutting insert on the end of the arm cuts a chip from the bar with approx. 395 m/min. After each cut, the chip was collected and the sample was weighed to calculate the chipped thickness through the steel's density and a geometrical description of the cutting edge's path in the bar (Fig. 2b).

After each cut, the insert was checked for breakouts or adhesions and, if necessary, turned to an unworn section of the cutting edge. During the cutting process, the passive force and cutting force were measured by dynamometers (Kistler). The energy consumed by the chipping was derived by integrating the cutting force signal over time. Furthermore, after every chipping, the consumed energy was calculated via the potential energies before and after chipping and the arm's rise angle. Cuts were conducted with cutting inserts RNGN090300 K68 (Prager GmbH), made of WC-Co with a diameter of 9.53 mm and a thickness of 3.18 mm and no clearance angle. Due to the geometrical conditions of the pendulum, the minimum uncut chip thickness was 0.05 mm since smaller thicknesses lead to an ironing of the material instead of cutting. A chip with constant thickness could only be obtained when a precut, was performed prior to the first experimental chip to establish a circular geometry of the bar top. The measured forces were corrected via a transmission filter that was established using an impulse hammer. The differently cut samples were given schematic names, consisting of the name of the heat treatment and the cutting depth (e.g. SA_0.2mm for the soft-annealed sample, cut with a depth of 0.2 mm).

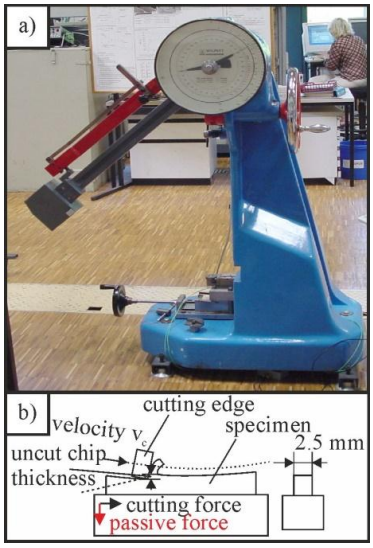

Figure 2. a) Single-pass pendulum and b) schematic of the chipping process.

C. Nanoindentation and Optical Analysis

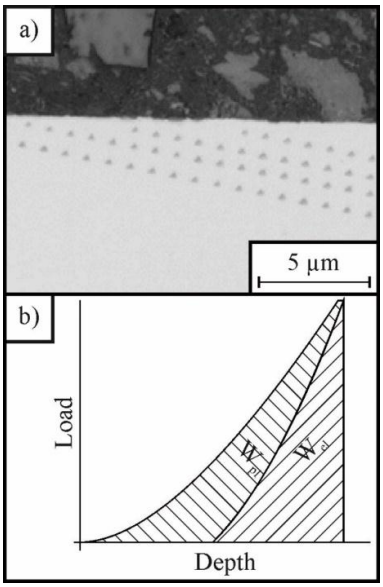

Figure 3. a) Scheme of nanoindentation and b) calculation of the elastic share from nanoindentation curves.

From the cut samples, smaller pieces were extracted out of the region around the middle of the bar and then cut in the middle lengthwise. The samples were then embedded in epoxy with the longitudinal middle plane as the examination plane so that possible microstructural changes underneath the cut surface could be examined. Starting from the cut surface, indentations with a maximum force of 10 mN were carried out into the bulk material for several µm with a Berkovich indenter (Fig. 3a) with an iMicro nanoindenter from Nanomechanics. The hardness and elastic modulus were calculated according to DIN EN ISO 14577 and OLIVER and PHARR [20]. Furthermore, the elastic share Wel/Wtot (Fig. 3b) was calculated from the indentation curves. This share represents the ratio between the elastic energy and the total deformation energy during an indentation process. Wtot is the total energy of the indentation process and consists of the elastic part Wel and the plastically deformed part Wpl.

Scanning electron microscopy examinations combined with EBSD measurements with an Oxford Instruments NordlysNano EBSD detector and a Tescan Mira 3 SEM were used to obtain a visual impression of microstructural changes underneath the cutting surface.

D. Residual Stress Measurement

Internal stress measurements were conducted with a µ360 portable X-Ray Residual Stress Analyzer (Pulstec Industrial Co., Ltd.) with the single incident angle X-ray exposure method (cosα-method) using a 0.3 mm collimator [21–24]. Cut bar samples were measured from the top of the bar down in the z direction to detect the residual internal stresses. A measurement of stresses at depths of several tens of micrometers was achieved by removing material by etching the cutting surface. A Lectropol-5 machine (Struers GmbH) with an A2 etchant (70 % ethanol, 12 % distilled water, 10 % 2-butoxy ethanol, 8 % perchloric acid), 12 volts etching voltage, and a maximum flow rate was used to remove material. In several trials with different exposure times, a constant rate of material removal was found to be valid in the relevant depths. The removal values were quantified by measurements using a confocal laser scanning microscope (CLSM) Keyence VK-X1000 that proved a uniform removal over the whole etching area. The CLSM indicated only minor edge rounding of the sample so that the focal point resided in a flat plateau, if placed in the middle of the bar. The measurements were conducted using CrKβ – radiation, emitted using a tube voltage of 30 kV at an angle of 35 °and a working distance of 39 ± 5 mm.

III. Results and Discussion

A. Cutting Experiments

Fig. 4 shows the cutting forces and passive forces of the differently heat-treated single-pass pendulum samples plotted against the uncut chip thickness. In the following, the approach to explain the deformation characteristics will include an analysis of the microstructure and chip formation.

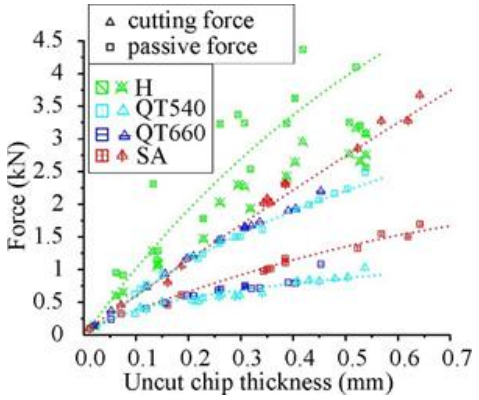

Figure 4. Measured forces from single-pass pendulum experiments.

A few considerable differences between the differently heat-treated samples are obvious. The highest cutting and passive forces are measured for the quenched-only samples, but they also deviate the most. The divergence of force values for the quenched samples is sometimes 1 kN. For the other heat treatments, the cutting forces are higher than the passive forces and the deviation is much smaller. The scatter of forces can be explained by an analysis of the chips. For small uncut chip thicknesses, all samples form coherent chips owing to the uniform deformation in the shear zone. Higher chip thicknesses tend to overextend the deformation abilities of the steel, which results in periodic piling up of material in front of the cutting edge and a separation along the shear zone, followed by a new pile-up. In this way, the typical sawtooth chips are formed. The transformation in chip-forming mechanisms occurs at relatively low chip thicknesses with the quenched samples because they have the smallest deformation tolerance and tend to deform by means of unstable and less predictable processes such as breaking and crack growth instead of shearing and localized plastic deformation. This instability in deformation leads to scattering of measured force values. Furthermore, the passive and cutting forces are nearly the same for smaller cutting depths, but for greater depths, the passive force increases above the cutting force. This is because the energy consumption for crack growth and breaking is smaller than for shearing. Additionally, the hardened specimens proved to be the most brittle ones in the tensile tests. Forces are slightly higher for the soft-annealed variant, despite it having lower strength in the quasistatic tensile tests (Table I). From an energetic point of view, the specific energy that is consumed during a tensile test equals the area under the stress/strain curve. This energetical tendency is also valid for chip formation, and from the quasistatic tests it is known that the SA samples yield low stresses, but the strain is considerably higher and deformation is more ductile. This could be an explanation for a similar force level of hardened and soft-annealed samples at small chip thicknesses. In this work, results from tensile tests are used to explain the overall deformation behavior, but it has to be considered at all times that the strain rates are not comparable to those in machining. The deviation of curves from approx. 0.3 mm chip thickness is a direct consequence of the aforementioned transition of chip formation mechanisms. The QT variants deform less uniformly and with more breaking shares from the same depth on, whereas the SA chips are uniform und coherent for higher thicknesses. This results in smaller energy consumptions for QT chip formation from middle chip thicknesses and thus in a flattening of the force curves, whereas the SA curves show uniform and hence predictable course of chip formation.

B. Nanoindentation

A possible influence of the cutting process on the microstructural properties was investigated by nanoindentation. Longitudinal cuts were made from the single-pass pendulum samples and orthogonal cutting samples were created and indented. Fig. 5 shows the hardness measured from the cut surface into the bulk material of QT540 single-pass pendulum samples that were cut with different uncut chip thicknesses and subsequently prepared.

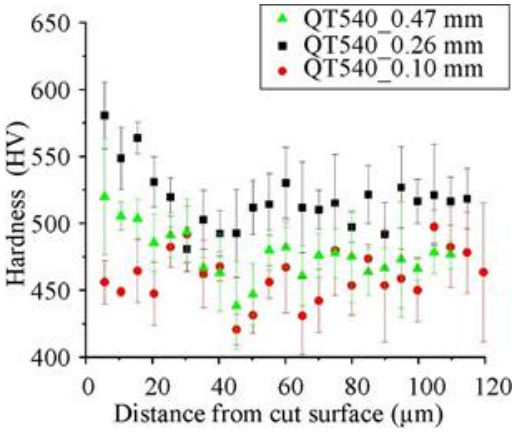

Figure 5. Subsurface hardness from nanoindentation of QT540 samples cut at different depths.

The hardness of the sample that was cut to a depth of 0.26 mm increases from around 520 HV in the bulk to approx. 580 HV in the first 40 µm from the cut surface. Between the bulk and the surface, there is a small decrease in hardness. The same hardness profile with a decrease from approx. 520 HV on the surface and approx. 460 HV in the bulk is measured with the sample that was cut with an uncut chip thickness of 0.47 mm. That curve also shows a considerable decrease in hardness of approx. 20 HV between the bulk hardness and the ramp towards the surface. The bulk hardness is reached further away from the surface than for the sample that was cut less deeply. The hardness of the sample that has been cut to a depth of 0.1 mm does not increase towards the surface. This implies an influence on the subsurface material by cutting that – in its depth and order of magnitude – is governed by the cutting depth. The general course of the graph is also reflected by the course of the elastic share (Fig.6). At the surface, the elastic share is higher than in the bulk material and between the bulk's elastic share and the increase towards the surface, a decrease in the elastic share can be seen that is deepest for the QT540_0.47mm sample. The increase in the elastic share signifies a strengthening in the regions underneath the surface because the material deforms during indentation testing elastically to a greater degree – i.e. it has a higher yield strength. The elastic share also maps the small decrease in hardness before the increase towards the surface that was discovered in hardness testing. This weakening is slightly stronger and deeper inside the bulk material for the more deeply cut sample. Hardness measurements for all the different heat treatments are presented in Fig. 7. The samples H, QT540, and QT660 were cut to similar cutting depths of around 0.3 mm and the soft-annealed sample was cut at 0.16 mm. The hardness profiles show distinct differences between the differently heat-treated microstructures. The SA sample was cut with half the cutting depth of the QT660 sample, and both show the same increase in hardness from the bulk to the surface.

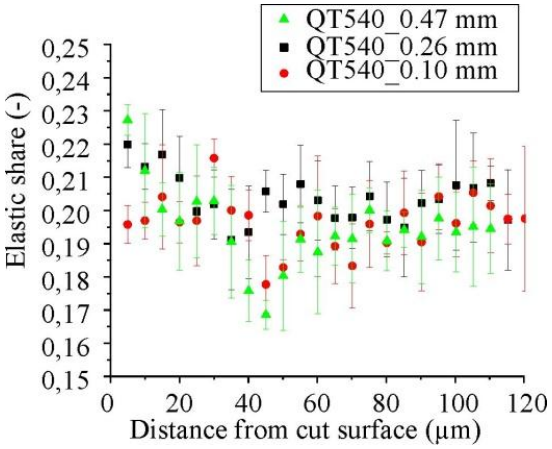

Figure 6. Subsurface elastic share from nanoindentation of QT540 samples, cut at different depths.

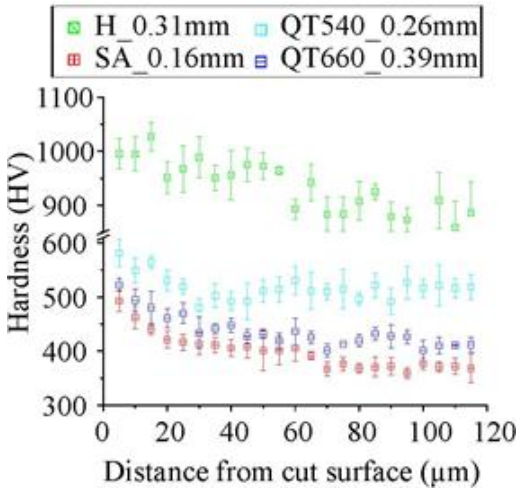

Figure 7. Hardness from nanoindentations of differently heat-treated samples.

The SA hardness graph shows a steady decrease until the bulk hardness is reached, whereas the QT660 indicates a small decrease in hardness that might also be the previously noticed hardness dent or a scatter in measurement. The bulk hardness is measured at a depth of approx. 60 µm for SA and QT660, which indicates that the influence of the cutting process is not equal for every microstructure because the cutting depths were so different. The softer and less strong SA sample strain hardens much deeper than the QT samples at equal cutting depths. This trend is supported by the hardness graphs of QT540 and H that, for cutting depths in the same range, are influenced less, and the hardened sample could even be called uninfluenced because the hardness indeed decreases over the measured distance from the surface; however, the decrease is so small that it could also be caused by scattering. Either way, the hardened sample, in particular, has to be examined as an optical analysis to clarify whether the microstructure has been affected in the same way as the differently heat-treated samples. The nanonindentation made it clear that an influence of cutting on the cut workpiece is present and is governed by the microstructure and thus the heat treatment and the depth of cut. To clarify the participating mechanisms, the microstructure after the cutting process needed to be analyzed.

C. Optical Analysis

SEM images of the longitudinal cuts were taken to analyze how the chipping process alters the microstructure and which mechanisms are responsible for the change. Fig. 8 shows SEM images of differently heat-treated samples. Fig. 8a shows the microstructure of QT540_0.26mm and reveals a sheared martensitic structure. The image highlights the shearing direction, which follows the cutting direction – from left to right – and is apparently existent in the entire image, but is more distinct near the surface and fades towards the bulk. The martensitic blocks seem to follow the shearing direction, and blocks are smaller and potentially divided in the top few micrometers. The topmost layer of several hundredth of nanometers exhibits only a few microstructural features, such as nearly horizontal lamellae, but otherwise seems to be featureless. Fig. 8b shows the microstructure in an SEM image of SA_0.16mm. Since the soft-annealed microstructure does not consist of lamellae, the shearing can only be detected by observing the annealing carbides that are aligned in lines along the cutting direction. The topmost layer of the SA sample seems to be severely deformed, but it could not be described as featureless. The microstructure of the QT660_0.39mm (Fig. 8c) also has a severely deformed layer on top, and the leftover martensite lamellae and the tempering carbides align along the shearing direction.

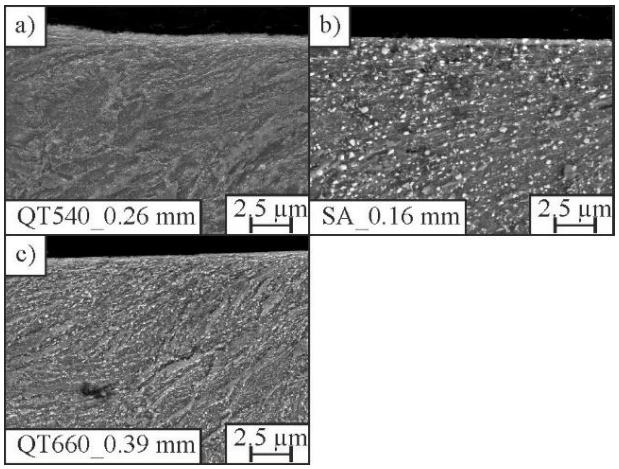

Figure 8. SEM image of the subsurface microstructure of differently heat-treated samples.

Fig. 9 shows EBSD images taken from single-pass pendulum samples in a region of 40 µm * 40 µm underneath the surface. In all images, the cutting direction was from left to right. Fig. 9a, 9b, and 9c are images of QT540_0.26 mm, QT540_0.47 mm, and QT660_0.39 mm, respectively. Analogously to the SEM images in Fig. 8, the sheared microstructure can be seen in the EBSD images. Grains are elongated and distorted in the cutting direction (Fig. 9a and 9b) and a grain refinement is visible. The grain refinement increases

towards the top, and whereas the grain size in the bulk is a few micrometers, the top layer consists of grains of about one hundred nanometers. It is obvious that the small grains were part of larger grains before cutting took place. The color encoding clearly shows that several small grains of one color were part of a larger grain. The assumption can be made that the grains were reoriented in the cutting direction and were split into smaller grains due to the high shear deformation in the topmost layer. The same has also been shown to be valid for splitting of carbides. In the first few hundred nanometers under the surface, the indexation of the EBSD signals failed in some regions. When a grain was smaller than the step size for the EBSD image of 500 nm, it is unlikely to be indicated correctly. As the indentation results suggested, the depth of the altered microstructure depends on the cutting depth. Samples QT540_0.26mm and QT540_0.47mm (Fig. 9a and 9b) reveal changes at a depth of approx. 20 to 30 micrometers, which is in agreement with the magnitude of the subsurface alteration detected by nanoindentation. CIHAK-BAYR et al. [25] suggested that the nanoindentation hardness/depth distribution gives a good first indication of the modified zone, but could underestimate its extent. For our study, it seems that the estimation with indentation was quite accurate. The grain refinement is one explanation for the strengthening in the surface region. The Hall-Petch relationship describes the strengthening of materials with grain refinement in a well-known equation. Until a critical grain size is reached, where the inverse Hall-Petch relation is valid and the material weakens with decreasing grain sizes, there is an increase in strength for smaller grains. The critical grain size that terminates grain-boundary strengthening is supposed to be around 20 nm to 50 nm [26]. This might not be reached by cutting tests, and a weakening of the material can only be proven several tens of micrometers into the material by nanoindentation, where the EBSD shows normal sized bulk grains. A second explanation for the increase in strength are the large plastic deformations in the near-surface areas. Many dislocations, the bearers of plastic deformation, are generated and remain in the material after cutting, which causes work hardening due to an increase in dislocation density. Additionally, the microstructural evolution is dependent on the microstructure prior to the cutting experiment. Fig. 9e shows a sheared and refined microstructure up to approx. 60 micrometers under the surface. The first few micrometers could not be indicated because of either the high dislocation density inside the grains or the small grain size. Although the cutting depth was only 0.16 mm, the alteration reached deeper than in all QT540 samples, regardless of the cutting depth. The cutting forces for the same uncut chip thicknesses of SA and QT540 samples were relatively identical (Fig. 4), but that obviously did not provide information about how the microstructure is affected. The soft-annealed microstructure has the smallest hardness and strength and thus it deforms more when it is subjected to the same loads. Additionally, the SA microstructure has the highest strengthening potential, i.e. that it is able to strengthen to a much greater extent through work hardening and grain-boundary hardening than the other microstructures. All the changes in the microstructure are caused by the two main factors – temperature and deformation – and they cause hardening and softening mechanisms at the same time, but at different depths the dominating mechanisms changes. The hardening by grain refinement and work hardening was already suggested in this study, but the literature discusses several more mechanisms. In cutting experiments, or similar setups, researchers observed white etching areas that develop through strain localization. Due to the very small grain size in the range of 30 to 500 nm [13], the areas appear to be featureless and white after etching. In addition, the question is often discussed whether the layers are formed by transformation or deformation, which also includes the question of how high the temperature was in the region of interest. Due to the analogies to adiabatic shear bands, these topics are mixed in the literature [14]. The microstructure in the SEM images of single-pass pendulum samples do show very small grains, but a featurelessness of a zone could not be observed. The main mechanisms for a refinement that are discussed in the literature are recovery and splitting of grains and carbides. The description of the microstructures observed in this work is in agreement with what can be found in the literature [13,14,25,27,28]. The same microstructural alterations and white layers were observed in pearlitic[8], martensitic, and bainitic structures. Suggestions have been made that the combined effect of temperature und rubbing of the tool on the surface is responsible for white layer formation and evolution of the microstructure. The effect of tool wear and resulting higher contact areas and more thermal and mechanical impact has been proven to enhance the refinement and encourage white layer formation [13]. The enormous plastic strains inside the material trigger a dynamic recovery that is aided by the temperature as a driving factor [13,28,29]. The existence of white layers with nanocrystalline structures on railway tracks, where the temperature during deformation is well below the austenization temperature, disqualifies the theory that these structures could only occur through decomposition of carbides and rehardening [25,29]. It does indeed strengthen the theory that the hardness towards the surface increases due to grain refinement. Also others suggest that the thermal diffusion, as a limiting factor in microstructural transformation, was too slow to enable reaustenization of near-surface areas [14]. It is assumed that, in this experiment, there was no phase transformation because the temperature might not have been high enough for the time required for austenization of the first micrometers of the sample. Additionally, the phase contrast of EBSD images shows that the amount of Fe_3C is the same in the bulk and underneath the surface. In the literature, it is suggested that austenization is always accompanied by dissolution of carbides, which cannot be confirmed at this point.

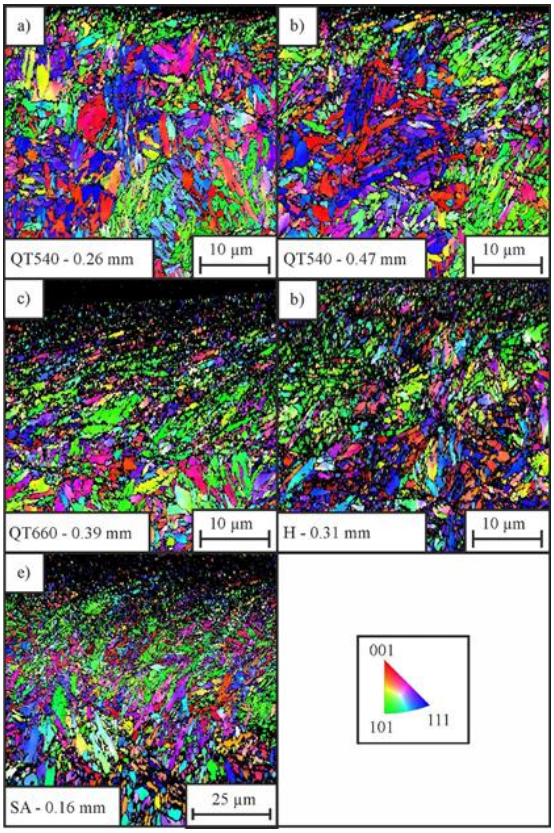

Figure 9. EBSD images of subsurface areas of different single-pass pendulum samples.

Underneath the topmost layers of similarly deformed samples, some researchers found layers of overtempered martensite (OTM) that had a lower hardness than the bulk [13,30]. In this work, we found a small decrease in hardness underneath the refined layer in the QT540 samples and hints of this feature in QT660 samples. It is possible that the thermal input from the cutting experiments was sufficient to temper the QT540 samples and reduce their hardness noticeably. This would indicate a cutting temperature of over 540 ℃ on the surface and thus a weakening effect on the refined structure that might be even harder when the tempering effect was smaller. In conclusion, in one sample, the weakening and strengthening forces operate simultaneously. On the very top, the refinement had a greater influence and an increase in hardness can be achieved if the microstructure has the strengthening potential. For instance, the H samples did not exhibit much influence because their microstructure was too resistant against the plastic deformation and a strengthening potential is not present. The QT samples exhibit a refinement on the top, where the mechanical mechanisms are dominant, and a decrease in hardness underneath where the tempering dominates. The soft-annealed sample is very susceptible to mechanical alteration of its microstructure and thus the refined area is quite large. Tempering is not possible and so this mechanism does not occur for the SA samples.

D. X-ray Analysis

Hypothesizes about the alteration of microstructures can be checked by analyzing residual stresses. The X-rays penetrate only a few micrometers into the material and thus deliver a stress value for only one spatial direction. The stresses were measured in and against the direction of cutting in the worn bar of the single-pass pendulum sample QT660_0.39mm. The measured stresses in both directions were averaged to obtain a general stress value on the analyzed surface. The internal stresses are shown in Fig. 10 as a function of the distance from the surface. The measured stress state is generally compressive and reaches approx. 160 µm into the material. The standard deviation for the first measurements is rather large, which might be caused by the rough and irregular surface. Also – of course – there must be tensile stresses somewhere to compensate the measured compressive stresses. Other researchers found that the stresses directly at the surface are tensile after cutting operations due to shearing in the cutting direction, the expansion and subsequent hindered contraction of the topmost material [19]. It is possible that the surface was not appropriate for stress measurements until the first few etching steps had smoothed the surface. The compressive stresses that are measured several tens of micrometers into the material indicate that the influence in the material was even greater than that suggested by the nanoindentation and the EBSD scan. The X-ray analysis provides a better view of the features involved in microstructural alteration that cannot be captured using optical methods or mechanical testing, and it sets a scale of how far the effect of temperature and deformation extended into the material.

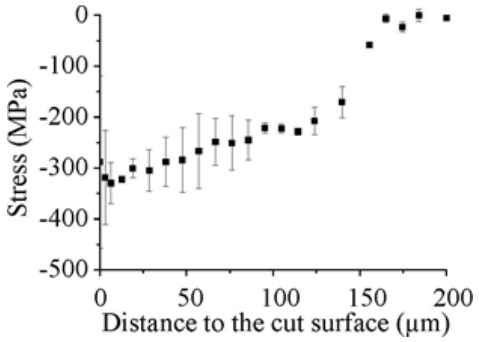

Figure 10. Measured residual stresses in the QT660_0.39mm sample.

IV. Conclusion

Single-pass pendulum tests with different cutting depths were conducted with differently heat-treated samples of low-alloyed tempering steel 42CrMo4. During the tests, the forces were measured and afterwards longitudinal cuts from several samples were investigated with nanoindentation and scanning electron microscopy, including EBSD analysis. Particular attention was paid to the question of microstructural evolution through the cutting process and the differences in structural alteration in the various microstructures. To complement the conclusions, internal residual stresses were measured with X-ray diffractometry. The following conclusions can be drawn:

- Even though different microstructures show similar cutting forces during experiments, the

alteration in the subsurface microstructure can be drastically different. The microstructure was found to be one of the major influences on the constitution of a cut sample. The strengthening potential of a microstructure is a decisive factor that determines the hardness and strength and thus the stress state underneath the surface. The heat-treatment history of a sample is decisive for the interaction of hardening and softening mechanisms and in which regimes which mechanism dominates. Also, the interaction with grain refinement needs to be considered, and it was not possible to fully distinguish between every single influencing factor.

- Although large deformations were visible through SEM and EBSD, white layers were not discovered in the samples from single-pass pendulum tests. On the one hand, the temperature was not high enough to produce transformed white layers. On the other hand, it might be the lack of contact area due to the fresh tool states that inhibited white layer formation. As the cutting insert was never used twice for cutting, the conditions did not seem to be favorable for the formation of deformed white layers, even though there was no clearance angle and thus much rubbing on the surface.
- Nanoindentation in combination with SEM and EBSD analysis was proven to be a powerful means to identify microstructural alterations. The measurement of residual stresses with a mobile X-ray diffractometer is a convenient means to quantify the degree of distortion in the grains. This enables a connection to be drawn between optical methods and the constitution of the crystal lattice. Although the surface condition was not ideal for the stress measurement with X-rays, it was possible to quantify the influence depth of features that cannot be captured by optical or mechanical testing. Future investigations should be carried out with a particular focus on a smoother surface state to be able to use the full functionality of residual stress measurements with X-rays.

CONFLICT OF INTEREST

The authors declare no conflict of interest.

AUTHOR CONTRIBUTIONS

Conceptualization, J.K.; investigation, J.K.; resources, J.K., F.P., P.W., W.T.; writing-original draft preparation, J.K.; writing-review and editing, J.K., F.P., P.W., W.T. All authors had approved the final version.

ACKNOWLEDGMENT

The investigations are based on the research project "Virtual Machining" (PE-216-0024), which is kindly funded by the Stiftung Mercator and the Mercator Research Center Ruhr.

The authors would like to thank the Center for Interface-Dominated High Performance Materials (Zentrum für Grenzflächendominierte Höchstleistungswerkstoffe, ZGH) at the Ruhr-Universität Bochum for the use of the CLSM.

REFERENCES

[1] Y. Altintas, P. Kersting, D. Biermann, E. Budak, B. Denkena, I. Lazoglu, "Virtual process systems for part machining operations," *CIRP Annals*, vol. 63, pp. 585–605, 2014.

[2] S. B. Wang, L. Geng, Y. F. Zhang, K. Liu, T. E. Ng, "Cutting force prediction for five-axis ball-end milling considering cutter vibrations and run-out," *International Journal of Mechanical Sciences*, 96-97 (2015) 206–215.

[3] B. Wu, X. Yan, M. Luo, G. Gao, "Cutting force prediction for circular end milling process," *Chinese Journal of Aeronautics*, vol. 26, 2013, pp. 1057–1063.

[4] P. Aristimuño, X. Lazcano, A. Sela, R. Basagoiti, P. J. Arrazola, "An optimization methodology for material databases to improve cutting force predictions when milling martensitic stainless steel JETHETE-M152," *Procedia CIRP 77*, 2018, pp. 287–290.

[5] S. Braun, M. S. rchak, H. C. Möhring, "Using model based analytic cutting force prediction in CAM toolpath generation," in *Procedia CIRP 82*, 2019, pp. 467–472.

[6] J. Sheikh-Ahmad, Y. He, L. Qin, "Cutting force prediction in milling CFRPs with complex cutter geometries," *Journal of Manufacturing Processes*, vol. 45, 2019, pp. 720–731.

[7] Q. Yao, M. Luo, D. Zhang, B. Wu, "Identification of cutting force coefficients in machining process considering cutter vibration," *Mechanical Systems and Signal Processing*, vol. 103, 2018, pp. 39–59.

[8] Y. Todaka, M. Umemoto, S. Tanaka, K. Tsuchiya, "Formation of nanocrystalline structure at the surface of drill hole in steel," *Mater. Trans*. vol. 45, 2004, pp. 2209–2213.

[9] J. Kundrák, Z. Gácsi, K. Gyáni, V. Bana, G. Tomolya, "X-ray diffraction investigation of white layer development in hard-turned surfaces," *Int J Adv Manuf Technol*, vol. 62, 2012, pp. 457–469.

[10] A. Ramesh, S. N. Melkote, L. F. Allard, L. Riester, T. R. Watkins, "Analysis of white layers formed in hard turning of AISI 52100 steel," *Materials Science and Engineering: A*, vol. 390, 2005, pp. 88–97.

[11] S. P. Trindade, K. H. S. Silva, D. A. Oliveira, A. M. Abrao, "Surface and subsurface alterations induced by hard turning of AISI 52100 bearing steel," *Journal of Engineering Science and Technology 13*, 2018, pp. 2765–2778.

[12] L. Chen, B. L. Tai, R. G. Chaudhari, X. Song, A. J. Shih, "Machined surface temperature in hard turning," *International Journal of Machine Tools and Manufacture*, vol. 121, 2017, pp. 10–21.

[13] S. Akcan, W. S. Shah, S. P. Moylan, S. Chandrasekar, P. N. Chhabra, H. T. Y. Yang, "Formation of white layers in steels by machining and their characteristics," *Metall and Mat Trans A* 33, 2002, pp. 1245–1254.

[14] J. Barry, G. Byrne, "TEM study on the surface white layer in two turned hardened steels," *Materials Science and Engineering: A* 325, 2002, pp. 356–364.

[15] N. Khanafi-Benghalem, E. Felder, K. Loucif, P. Montmitonnet, "Plastic deformation of 25CrMo4 steel during wear," *Wear 268* , 2010, pp. 23–40.

[16] S. J. Huang, V. I. Semenov, L. S. Shuster, P. C. Lin, "Tribological properties of the low-carbon steels with different micro-structure processed by heat treatment and severe plastic deformation," *Wear* , vol. 271, 2011, pp. 705–711.

[17] Q. Shen, Z. Liu, Y. Hua, J. Zhao, W. Lv, A. U. H. Mohsan, "Effects of cutting edge microgeometry on residual stress in orthogonal cutting of inconel 718 by FEM," *Materials* (Basel, Switzerland) 11 (2018).

[18] A. Singh, A. Agrawal, "Investigation of surface residual stress distribution in deformation machining process for aluminum alloy," *Journal of Materials Processing Technology*, vol. 225, 2015, pp. 195–202.

[19] S. Q. Wang, J. G. Li, C. L. He, R. A. Laghari, "An analytical model of residual stress in orthogonal cutting based on the radial return method," *Journal of Materials Processing Technology*, vol. 273, 2019, 116234.

[20] W. C. Oliver, G. M. Pharr, "An improved technique for determining hardness and elastic modulus using load and displacement sensing indentation experiments," *Journal of Materials Research*, vol. 7, pp. 1564–1583, 1992.
[21] K. Tanaka, "X-ray stress measurement by the cos method using two-dimensional detector part 2: Measurement procedure and applications // X-ray stress measurement by the cos α method using two-dimensional detector part 2: Measurement procedure and applications," *Journal of the Society of Materials Science*, Japan, vol. 66, 2017, pp. 479–487.
[22] K. Tanaka, JSME-TJ, "The cosα method for X-ray residual stress measurement using two-dimensional detector," *Mechanical Engineering Reviews*, vol. 6, 2019, 18-00378-18-00378.
[23] L. Spieß, R. Schwarzer, H. Behnken, G. Teichert, "Moderne Röntgenbeugung: Röntgendiffraktometrie für Materialwissenschaftler," *Physiker und Chemiker*, *Vieweg+Teubner Verlag*, Wiesbaden, s.l., 2005.
[24] S. Taira, K. Tanaka, T. Yamasaki, "A method of X-ray microbeam measurement of local stress and its application to fatigue crack growth problems," *Journal of the Society of Materials Science*, Japan, vol. 27, pp. 251–256, 1978.
[25] U. Cihak-Bayr, G. Mozdzen, E. Badisch, A. Merstallinger, H. Winkelmann, "High plastically deformed sub-surface tribozones in sliding experiments," *Wear 309*, 2014, pp. 11–20.
[26] S. H. Whang (Ed.), "Nanostructured metals and alloys: Processing, microstructure, mechanical properties and applications," Woodhead Pub, Cambridge, U.K, 2011.
[27] Y. K. Chou, C. J. Evans, "White layers and thermal modeling of hard turned surfaces," *International Journal of Machine Tools and Manufacture*, vol. 39, 1999, pp. 1863–1881.
[28] S. B. Hosseini, U. Klement, Y. Yao, K. Ryttberg, "Formation mechanisms of white layers induced by hard turning of AISI 52100 steel," *Acta Materialia*, vol. 89, 2015, pp. 258–267.
[29] S. B. Hosseini, T. Beno, U. Klement, J. Kaminski, K. Ryttberg, "Cutting temperatures during hard turning—Measurements and effects on white layer formation in AISI 52100," *Journal of Materials Processing Technology*, vol. 214, 2014, pp. 1293–1300.
[30] Y. B. Guo, A. W. Warren, F. Hashimoto, "The basic relationships between residual stress, white layer, and fatigue life of hard turned and ground surfaces in rolling contact," *CIRP Journal of Manufacturing Science and Technology*, vol. 2, 2010, pp. 129–134.

Janis S. Kimm, born in Hagen in 1991, received his Bachelor of Science in mechanical engineering from the Ruhr-Universität Bochum in 2015. He received the Master of Science in mechanical engineering from the Ruhr-Universität Bochum in 2017.
He works as an ASSISTANT RESEARCHER at the chair of materials technology at the Ruhr-Universität Bochum since 2017.